Flow Physics Explains Morphological Diversity of Ciliated Organs

Janna C. Nawroth[1,2,†], Feng Ling[1,2,†], Tara Essock-Burns[3], David Stein[4], Margaret McFall-Ngai[3,5,6], Kakani Katija[7], Michael J. Shelley[4,8], Eva Kanso[1*]

[1]Department of Aerospace and Mechanical Engineering,
University of Southern California, Los Angeles, California 90089, USA
[2]Helmholtz Pioneer Campus, Helmholtz Munich
- Deutsches Forschungszentrum für Gesundheit und Umwelt (GmbH),
Ingolstaedter Landstrasse 1, 85764 Neuherberg, Germany
[3] Kewalo Marine Laboratory, University of Hawaii at Manoa, USA
[4]Center for Computational Biology, The Flatiron Institute, New York, USA
[5] Pacific Biosciences Research Center, University of Hawaii at Manoa, USA
[6] Biology and Environmental Research Division, Carnegie Insitute, California, USA
[7]Monterey Bay Aquarium Research Institute, California, USA
[8]Courant Institute, New York University, New York, USA
[*]To whom correspondence should be addressed; E-mail: kanso@usc.edu.
[†]J.C.N, and F.L. contributed equally to this work.

Ciliated organs that pump luminal fluids are integral to animal physiology. Such organs, including the human airways and reproductive tracts, feature ciliated ducts that direct internal flows. Although cilia organization and duct morphology vary drastically in the animal kingdom, ducts are typically classified into two, seemingly disconnected, archetypes: the familiar carpet and the intriguing flame designs. The reason behind this dichotomy and how duct design relates to fluid pumping remain unclear. Here, we apply morphometric

and mechanistic analyses to ciliated ducts across all animal phyla. We find that two structural parameters, lumen diameter and cilia-to-lumen ratio, organize the observed duct diversity into a continuous spectrum that connects carpets to flames. Using a unified fluid model, we discover that carpets and flames, respectively, maximize flow rate and pressure generation, which is consistent with physiological requirements for bulk transport and filtration, whereas intermediate designs along the morphological spectrum constitute optimally efficient hybrids. We propose that convergence of ciliated organ designs follows functional constraints rather than phylogenetic distance, and we present universal design rules for ciliary pumps.

Introduction

To perform their physiological functions, many organs in animal biology rely on luminal flows driven by the coordinated beat of motile cilia. In humans, ciliated ducts (CDs) pump fluids in the airways [1], brain ventricles and spinal canal [2], and reproductive system [3]. Their failure is directly linked to major pathologies, including bronchiectasis [5], hydrocephalus [6], and ectopic pregnancy [7]. Cilia in these ducts are usually short relative to the lumen diameter and are oriented perpendicular to the epithelial surface, in a ciliary carpet design [8]. Many animals also feature ducts with a strikingly different cilia arrangement, the ciliary flame design [9], where tightly packed, comparatively long cilia beat longitudinally along a narrow lumen. Ciliary flames that are thought to pump fluid for the purpose of excretion provide a model system for studying human kidney disease [10, 11].

Despite the fundamental importance of CDs in animal physiology, functional studies of intact CDs are rare [12, 4], and the relationship between CD morphology and their ability, or failure, to pump fluid remains largely unexplored. Ciliary flames and carpets have not been

compared functionally, nor have other CD morphologies been characterized in relation to these two fundamental designs.

Existing studies focused on exposed ciliated surfaces and externally ciliated organisms because it is difficult to measure ciliary beat and fluid flow in intact internal ducts. Cilia oscillations, metachronal coordination, and microscale flows have been observed in microdissected *ex-vivo* epithelia [13], engineered *in-vitro* tissues [14, 15], and, more recently, in organ-on-chip models [16, 17]. Additionally, leveraging the remarkable conservation of the ultrastructure of motile cilia among eukaryotes, diverse protist and animal model systems have emerged for probing the functional spectrum of cilia, from locomotion and feeding [18, 19] to symbiotic host-microbe partnerships [20, 21]. Current consensus from experimental and theoretical evidence is that coordinated metachronal waves are prominent features of ciliary carpets [14, 22–24], emerge spontaneously through hydrodynamic and substrate interactions [24–28] and dominate mechanisms of directional fluid transport [24, 29–32]. Ciliary carpets with no coordinated waves appear to be the exception and have been associated with fluid mixing as opposed to directional fluid pumping [4, 20]. External cilia that beat longitudinally in solitary or pairwise configurations, such as in mammalian sperm cells or in the unicellular protozoa *Euglena* and alga *Chlamydomonas*, are often called eukaryotic flagella and drive motility and gait transition in these microorganisms [19, 33–35]. But when longitudinally-beating cilia occur internally in a bundle, such as in *Planarians*, they are labeled as ciliary flames, and are thought to be associated with filtration [9–11].

Despite remarkable progress in understanding the functional diversity of cilia, to date, the architecture of intact CDs inside of organisms is yet to be related to their pumping performance. Establishing this connection would elucidate the apparent dichotomy between carpets and flames, inform our understanding of human ciliopathies [36], aid in comparing different internal fluid transport mechanisms in animals [37, 38], and help in assessing the hypothesized

roles of CDs in excretion [10, 11] and host-microbe interactions [39].

In this study, we leverage two giant larvaceans (*Bathochordaeus stygius* and *Bathochordaeus mcnutti*) as powerful model systems to study intact CDs. Larvaceans belong to Tunicata (Urochordata), a sister clade of vertebrates, and are an emergent model system for the study of gene regulation, chordate evolution, and development [40]. Giant larvaceans feature a multitude of ciliated ducts with both carpet and flame designs with exceptional optical access [41, 42], providing uniquely ideal conditions for studying the fundamental properties of cilia-generated flows in intact CDs with direct relevance to other chordates including humans.

To derive universal structure-function relationships, we combined our functional studies in giant larvaceans with an exhaustive review of published CDs in animals, and with physics-based computational models. Specifically, we (i) studied the larvacean system to characterize the morphological features and fluid transport mechanisms in flames versus carpets. We then used these insights to (ii) conduct a morphometric analysis of CDs across all animal phyla and identify a two-dimensional (2D) morphospace that organizes the design of CDs by fluid transport function, and to (iii) explain this structure-function relationship through a unifying physics-based model that links duct morphology to fluid pumping in terms of flow rate and pressure generation. We arrive at a functional assessment of CDs based on morphology that could aid in studying their role in human disease as well as inspire engineering applications [43–45].

Results

Ciliary carpet versus flame duct designs

Microscopic inspection revealed that most ciliated ducts in giant larvaceans, such as in the pharynx, esophagus and gut, exhibit the ciliary carpet design associated with mucus clearance and fluid circulation in humans [46] (Fig. 1A). The ciliary flame design, which is associated

with filtration in planarians [10], was found in the giant larvaceans' prominent ciliated funnel (Fig. 1A and S.1), an organ whose function remains obscure [47]. To compare and contrast carpet and flame designs, we measured their structural properties, ciliary activity, and fluid transport velocity in the intact animal. In the carpet-style esophagus, cilia are much shorter than the width of the lumen (ca. 6 μm vs. $100 - 200$ μm, respectively) (Fig. 1B) and they beat at ciliary beat frequencies (CBF) of 20 Hz with a stroke cycle perpendicular to the duct walls (Fig. 1D). Neighboring cilia coordinate their beat in metachronal waves that propagate longitudinally along the duct, propelling luminal fluid and food particles at flow speeds of up to 50 μm s^{-1} (Fig. 1C, Suppl. Movie 1). The ciliary beat frequency and flow parameters are comparable to those of other ciliary carpets, such as the mammalian airway and ependymal epithelia [2, 48].

In contrast to the carpet-style esophagus, cilia in the larvacean funnel are longer than the width of the duct lumen (ca. 100 μm versus 55 μm, respectively) and align parallel to the lumen in a densely packed fashion (Fig. 1E and S.1B-D), which is typical of ciliary flames associated with filtration [9, 11]. While the beat kinematics of most ciliary flame systems are unknown, our data suggested that the coordinated motion of the many parallel cilia create periodic waves that travel along the entire length of the 100 μm long larvacean flame (Suppl. Movie 2), demonstrating similar kinematics as the better studied, 20-times shorter ciliary flames of planarians (Fig. S.2B) [49]. The longitudinal traveling waves thus appear to be a key feature of ciliary flames regardless of size and, from the perspective of their action on the surrounding fluid, are reminiscent of the metachronal waves in ciliary carpets (Fig. S.2). The larvacean ciliary flame beats at a CBF of up to 60 Hz (Fig. 1g), which falls into the upper range observed in ciliary carpets [50], and generates equally comparable flow speeds of ca. 40 μm s^{-1} towards the internal blood sinus (Fig. 1F, Suppl. Movie 3).

Taken together, our data suggested that despite their structural and reported functional dif-

ferences, both ciliary carpet and flame ducts generate unidirectional flows by leveraging the same active fluid transport mechanism, namely, the use of coordinated ciliary waves. Indeed, in ciliary carpets, metachronal wave coordination emerges spontaneously and dominates fluid transport [24, 29–32], but fluid transport in ciliary flames is less understood. The stark structural differences between ciliary carpets and flames and the apparent lack of other CD designs in larvaceans underscore the questions of whether all ciliated ducts in nature fall into one of these two design categories and what the functional consequences are.

Comparative morphometric analysis suggests functional constraints on duct designs

To address these questions we performed an exhaustive survey on the presence, morphology, and reported fluid transport functions of CDs in all 34 animal phyla [51, 52]. Since kinematic data of ciliary beat was unavailable in most cases, we collected morphometric data accessible from still images of CDs, namely, cilia orientation relative to duct (perpendicular or longitudinal), duct length L, duct diameter H, cilia length $h/2$, and cilia-to-lumen ratio h/H, which ranges from 0 to 1 and represent the relative fraction of the duct taken up by cilia, independent of cilia orientation (Fig. 2A and Fig. S.3). We collected these data from published work and our own imaging analysis of multiple species of Urochordates and Mollusks (Fig. S.4), covering a total of 58 duct systems representing 26 animal phyla (Table S1). The remaining 8 phyla either lacked evidence of motile cilia or CDs or, in the case of sponges (phylum Porifera), were excluded because of their complex duct morphologies [53, 54].

Using a cross-validated machine learning approach, we probed the ability of the morphometric parameters to correctly predict whether a given ciliated duct was reported to perform bulk transport (clearance, circulation, or cargo transport) or serve as a filter/valve. We found that the cilia-to-lumen ratio h/H was a perfect predictor of known CD function and, when plotted

against lumen diameter H to visualize the spatial scales involved, organized the 58 surveyed duct systems by function (Fig. 2B and Fig. S.5). A value of h/H >0.62 was associated with filtration or valve function, and a value of h/H <0.62 indicated bulk fluid transport, clearance, and mixing. Mapping cilia orientation onto the morphometric distribution further showed a clear association of filtration/valve function with flame designs (longitudinal cilia and high values of h/H) and of bulk transport with carpet designs (perpendicular cilia and low values of h/H). Cilia orientation by itself, however, was not an optimal predictor of function due to marked exceptions, such as longitudinally aligned (but sparse) cilia in the collecting ducts of planarian excretory organs, which perform bulk transport of fluid [9]. Other morphometric parameters, e.g., duct length or diameter, were at best weakly predictive of CD function (Fig. S.6).

The h/H against H plot showed a continuous distribution of designs spanning carpets to flames, rather than a strict dichotomy. CD designs can thus be described by their unique combination of cilia-to-lumen ratio and lumen diameter. In general, higher cilia-to-lumen ratios tended to associate with narrower ducts (typically flames), and lower cilia-to-lumen ratios with wider ducts (typically carpets), whereas systems with large H and large h/H, for example, were markedly absent. As the distribution of systems in the morphospace was not reflected by their phylogenetic distance (Fig. 2 B, C and S.5) but organized by their fluid transport activity, these data suggest a convergent evolution of CD designs based on function.

Intuitively, the design of CDs for fluid pumping is constrained by the metabolic cost of building and actuating the cilia [55, 56], limiting the number and length of cilia on a given ciliated surface. A higher cilia-to-lumen ratio h/H also implies that less space in the duct lumen can be taken up by fluid. Minimizing the cost of cilia production along a cell surface and the cost of cilia activity while maximizing fluid volume seems to favor a low cilia-to-lumen ratio at large lumen diameter. However, the flame cells observed in purported filtration systems suggest that other functional considerations are at play. Specifically, structural data suggest

that flame cells achieve filtration by pumping fluid through a flow-resisting sieve [9, 57, 58], indicating that higher cilia-to-lumen ratios may be specialized to pump fluid in the presence of high resistance to flow, or, equivalently, in the presence of *adverse pressure gradients* that cause counter-currents relative to the desired flow direction.

We hypothesized that lower cilia-to-lumen ratios (typically carpets) which transport fluids at comparatively greater lumen diameters and flow rates, are able to pump flows at low or zero adverse pressures, whereas higher cilia-to-lumen ratios (typically flames) are limited to small diameters and low flow rates because of the high density of active ciliary material required to overcome adverse pressure gradients. These trade-offs would explain both the non-uniform distribution of CD designs and their functional classification.

A unified model of fluid transport in ciliated duct designs

To rigorously probe this hypothesis, we developed a computational model that compares fluid transport in CDs with different combinations of lumen diameter H and cilia-to-lumen ratio h/H.

Our model represents the ciliated portion of the duct as an active porous medium, described by the Brinkman-Stokes equations, lining a fluid-filled channel (Fig. 3A and Suppl. Methods §S.2). Ciliary motion is implemented as density waves that mimic the metachronal and traveling waves observed in carpets and flames. The proposed model bridges these two archetypes in a concise way that is unachievable using existing envelope [13, 60–64] and discrete cilia models [30, 65–71] and enables efficient exploration of the entire morphospace spanned by h/H and H independent of cilia orientation, including designs not (yet) known to biology. The number of cilia per unit duct length defines a cilia density $\rho_c(\mathbf{x}, t)$ that varies in space $\mathbf{x}$ and time t, with a uniform constant counterpart $\bar{\rho}_c$ in an undeformed reference configuration. The ciliary waves specify a velocity field $\boldsymbol{v}(\mathbf{x}, t)$ in these ciliated layers. These prescribed ciliary

waves, with interdependent $\rho_c(\mathbf{x}, t)$ and $\boldsymbol{v}(\mathbf{x}, t)$, drive the luminal fluid velocity $\boldsymbol{u}(\mathbf{x}, t)$ in the CD, including fluid that permeates the porous ciliated layers.

We focused on unidirectional ciliary waves, but our model is equally applicable to general beat patterns and ciliary waves (Suppl. Materials, §S.4). To compare CDs that demand the same growth and actuation costs of the ciliary layers, we considered ciliary waves with fixed amplitude a, wavelength L, and frequency ω, and we fixed the total ciliary material in the duct by setting $\bar{\rho}_c h$ to a constant, thus conserving the power input to the fluid. This conservation of ciliary material, $\bar{\rho}_c h =$ constant, is equivalent to a conservation of the ratio of cilia volume to duct surface area.

We next evaluated the performance of CDs with different combinations of lumen diameter H and cilia-to-lumen ratio h/H and constant ciliary material $\bar{\rho}_c h$ in terms of net flow rates Q, sustained adverse pressure ΔP, and overall pumping efficiency η [12, 59].

Higher cilia-to-lumen ratio generates higher pumping pressure

We first considered two systems with low cilia-to-lumen ratio ($h/H = 0.2$) and high cilia-to-lumen ratio ($h/H = 0.9$) and same lumen diameter $H = 100$ μm, and we set $\bar{\rho}_c h = 1000$, which is an upper bound of total ciliary material in all surveyed CDs (Fig. S.8). The low cilia-to-lumen ratio generated higher flow speeds at zero adverse pressure, but failed and allowed reversal of luminal flow in the presence of adverse pressure ΔP (Fig. 3A I and II), whereas positive luminal flow remained robust in the high cilia-to-lumen ratio (Fig. 3A III and IV). In fact, at zero adverse pressure, positive flows were generated by all cilia-to-lumen ratios h/H (Fig. 3B), except in the two limiting cases $h/H \to 0$ and $h/H \to 1$ (Suppl. Methods §S.2.8). Maximal flow speeds on the order of 100 μm s^{-1} were achieved at small h/H, consistent with experimentally observed flow speeds in airway epithelia [48, 72]. The high cilia-to-lumen ratio, by contrast, was more effective in maintaining positive flow speeds under adverse pressure for

a wide range of ΔP values (Fig. 3C); this agrees with the hypothesized filtration function of flame cells which involves fluid transport in the presence of adverse pressures [10]. Essentially, at $\Delta P = 0$, any CD design in the morphospace $(H, h/H)$ can produce positive flow (Fig. 3D), but at weaker speed U as the cilia-to-lumen ratio h/H increases for a given lumen diameter H. However, requiring a positive speed of $U = 100$ μm s^{-1} under adverse pressure gradually excludes CD designs with larger H and lower h/H as the adverse pressure gradient increases (Fig. 3E).

Optimal duct design depends on pressure requirements

This trade-off between net flows and sustained adverse pressure is best appreciated in the pump function space $(Q, \Delta P)$, where $Q = UH$ is the net flow rate (Fig. 4A). A ciliary pump $(H, h/H)$, for a choice of material constant $\bar{\rho}_c h$, operates along a characteristic curve connecting its maximal generated flow rate Q at $\Delta P = 0$ to the maximal adverse pressure ΔP sustained without causing flow reversal $Q = 0$. Each ciliary pump functions along its own characteristic curve, depicted in solid lines in Fig. 4A for representative designs with low and high cilia-to-lumen ratios, including those of the larvacean in Fig. 1. Intuitively, a ciliary pump performs best when operating near the transition from maximal flow rate to maximal pressure.

For the flame-type larvacean funnel, our results at these transitional values suggest that, when pumping in water with a CBF of $\omega = 60$ Hz, it can provide a maximal flow rate of about 1.5 μl hr^{-1} at $\Delta P \approx 1.4$ Pa μm^{-1}, which amounts to generating 230 Pa of pressure for the 160 μm long duct. In contrast, a similar calculation estimates that the carpet-type larvacean esophagus ($\omega = 20$ Hz) can provide a much larger flow rate of nearly 25 μl hr^{-1}, albeit against a weaker pressure of less than 0.1 Pa over its 2500 μm length.

To systematically probe optimal CD designs for pumping against adverse pressure under biologically-relevant limitations on ciliary material and power input, we introduced a pumping

efficiency η defined as the ratio of the rate of change of the fluid mechanical energy to the power input by the ciliary waves (Suppl. Methods §S.2.9-S.2.11). We maximized efficiency η over the entire morphospace $(H, h/H)$ for a wide range of adverse pressure gradients ΔP and at a fixed value of ciliary material $\bar{\rho}_c h$. We repeated the same process at different values of $\bar{\rho}_c h$ ranging from 1 to 1000 to reflect the entire span found in our morphometric survey (Figs. S.8B and S.13). Each value of $\bar{\rho}_c h$ represents a distinct level of power input. At each value within the empirically-derived range of $\bar{\rho}_c h$, optimal CD designs formed a line, shown in solid white and labeled by the corresponding value of $\bar{\rho}_c h$ in Fig. 4B,C. Each design on the line is optimal for a given maximal adverse pressure gradient. The maximal adverse pressure gradient sustained at each optimal design is shown in orange (Fig. 4B) and the corresponding flow rate in green (Fig. 4C). For the entire range of empirically-derived values of ciliary material $\bar{\rho}_c h$, optimal designs formed a foliation of lines spanning the entire spectrum from carpets to flame designs. Relatively large H and low h/H (typically carpets) are optimal for generating high volume flows against weak adverse pressure gradients while smaller H and high h/H (typically flames) are optimal for pumping fluids against stronger adverse pressure gradients albeit at lower flow rates (Fig. 4B,C). When displayed on the function space (Fig. 4A), optimal designs (dotted lines) are indeed located at the transitions from maximal flow rate Q to maximal adverse pressure ΔP.

Grey areas in Fig. 4B,C correspond to sub-optimal designs. Designs that have relatively small lumen diameter H and low cilia-to-lumen ratio h/H are sub-optimal because, at constant $\bar{\rho}_c h$ and weak ΔP, ducts with larger H are always more efficient in transporting flows at low h/H (Figs. S.11-S.14). Designs that have relatively large H and high h/H (grey area in Fig. 4B,C) are also sub-optimal because, at constant $\bar{\rho}_c h$ and strong ΔP, increasing the lumen diameter H lowers the density $\bar{\rho}_c$ of ciliary material (Fig. S.8A) and, in turn, the input power density, thus limiting the value of ΔP that can be sustained at high h/H, potentially leading to

flow reversal (Figs. S.11-S.14). Put differently, although increasing H at high h/H is theoretically viable, the required ciliary material and input power grow disproportionately and likely beyond biological limits.

Superimposing the biological data of Fig. 2A onto the map of optimized duct geometries (Fig. 4B,C), we found that all surveyed designs closely align with the lines that maximize pumping efficiency at different levels of power input, which excludes designs both in the small H, low h/H and in the large H, high h/H corners of the morphospace. Importantly, we found that systems whose primary function is to transport luminal fluid in bulk are typically ciliary carpets and thus reside in the region of the morphospace with larger lumen diameter H and lower cilia-to-lumen ratio h/H. Systems with presumed filtration functions are typically ciliary flames and occupy the region of the morphospace with smaller lumen diameter H and higher cilia-to-lumen ratio h/H characterized by the ability to sustain higher adverse pressure gradients.

Discussion

We established a quantitative link between the morphology and fluid pumping function of ciliated organs. Our analyses imply that the distribution of morphological features of ciliated ducts in nature is not accidental since each biological system in our survey is the optimal pump for operation at a specific pressure and flow rate. At the extreme ends of the spectrum, systems with cilia-to-lumen ratios near zero maximize flow rate whereas systems with cilia-to-lumen ratios near unity optimize pressure generation, consistent with the known roles of ciliary carpets in bulk transport and of flame cells in ultrafiltration, respectively. Notably, our study reveals that many systems exhibit intermediate cilia-to-lumen ratios and predicts that they may perform fluid transport against some resistance, for example, to maintain a hydrostatic head [73]. Our analysis also explains the absence of surveyed CDs in two quadrants of the morphospace because our model predicts such pump designs to be either comparatively inefficient, e.g., the same flow

rate would be possible at less power input, or unfeasible given likely biological limits on ciliary material and power input.

Given such morphology dependent fine-tuning of pump performance, we can now use structural features of a given CD to predict its relative ability to either transport fluids in bulk or to perform filtration. Case in point, our findings support the decades-old hypothesis that the larvacean's ciliated funnel (Fig. 1, Fig. 2a and Suppl. Movie 2) helps maintain the internal fluid volume through unidirectional injection of filtered seawater into the blood [74], rather than being limited to sensory and endocrine functions [47, 75, 76]. In the Hawaiian bobtail squid (*Euprymna scolopes*), we can predict that the ciliated conduit to the light organ that hosts the bacterial symbiont (*Vibrio fischeri*) transports fluids in the duct and antechamber, whereas filtration or pressurization may occur in the bottleneck region (Fig. S.4C-E). Importantly, the bottleneck diameter varies dynamically during different stages of colonization [39], suggesting a switch between filtration and clearance functions that could help maintain the host-symbiont association. Similarly, the ciliated pore canals of the madreporite in sea urchins appear to change dynamically between low and high cilia-to-lumen ratios (Suppl. Table 1), and our results support the proposed functional switch between fluid pump and valve that maintains the animal's inner hydrostatic pressure [73].

Our findings may provide general insights into the evolution of waste excretion strategies in animals and offer a functional explanation why ciliary flame-based excretory organs are abundant in animals not exceeding a few milligrams in body mass, whereas larger animals rely on blood pressure pumped by the muscle-powered heart [77]. Our study suggests two mechanisms. First, because cilia have limited length and emanate at finite density from the tissue surface, increasing the lumen diameter eventually lowers the cilia-to-lumen ratio and restricts the power input, thus limiting the pressure that can be sustained and the flow rate than can be generated by an individual flame pump. Second, scaling up flame-based filtration by the parallel operation of

many small flame units would require a much larger organ volume than a system that leverages the higher filtration fluid pressures achieved by the heart (Suppl. Methods §S.5). But even if we were to assume unlimited cilia length and lumen diameter, advantageous scaling of energy efficiency in muscle versus ciliated cells would also disfavor the emergence of extremely long ciliated flames and bias evolution towards muscle-powered pumps in larger animals.

Along with assessing the pumping function of healthy ciliated organs, our study may aid in the functional interpretation of disease phenotypes, such as narrowing of ciliated ducts [78], and inform the development of drugs that disrupt excretory functions of parasites [49]. Additionally, our approach provides a rational design tool for tissue-engineered and synthetic ciliary pumps and devices that perform filtration and flow control, in addition to existing carpet-like configurations for bulk transport [43–45, 79].

Our analysis does have limitations. Our survey might be missing alternative CD designs in the "hidden biology" of less studied animals [80]. We also omitted ciliated ducts whose geometry is not well described by our 2D morphospace, such as the ciliated chamber of sponges [53, 54, 81] and some of the unique ciliated spaces found in ctenophores [82–85]. No distinction was made between different types of fluids, such as mucus and water, and we did not consider mixing flows. We considered a Newtonian fluid model, heuristic cilia waveforms and material constraints, and fundamental measures of pumping performance in order to limit the number of variables and reveal the dominant structure-function relationships of ciliated ducts. We demonstrated that our model robustly captures leading order effects of ciliary fluid pumping without requiring implementation of detailed cilia kinematics. Hence, limitations notwithstanding, our 2D morphospace and functional map are representative and relevant for the majority of ciliated ducts known to biology and provide a universal tool for assessing the physiological role and integrity of ciliated organs.

Funding

This work was funded by NSF Inspire grant MCB1608744 (E.K. and M.M.-N.), NIH R01 HL153622 grant (E.K. and J.N.), NIH R37 AI50661, COBRE P20 GM125508, OD11024 and GM135254 grants (M.M.-N.), DMR-2004469 (M.J.S.), and David & Lucile Packard Foundation (K.K.). Acquisition of the Leica TCS SP8 X confocal microscope was supported by NSF DBI 1828262 (M.M.-N.).

Authors contributions

Janna Nawroth: Conceptualization, Investigation, Methodology, Formal Analysis, Software, Data curation, Writing- Original draft preparation, Reviewing and Editing. Feng Ling: Investigation, Methodology, Formal Analysis, Software, Data curation, Validation, Visualization, Writing- Original draft preparation, Reviewing and Editing. Tara Essock-Burns: Investigation, Visualization, Writing - Reviewing and Editing. David Stein: Methodology. Margaret McFall-Ngai: Writing - Reviewing and Editing, Funding acquisition. Kakani Katija: Methodology, Investigation, Resources, Writing - Reviewing and Editing. Michael Shelley: Methodology, Writing-Reviewing and Editing. Eva Kanso: Conceptualization, Investigation, Methodology, Formal Analysis, Writing- Original draft preparation, Reviewing and Editing, Supervision, Funding acquisition.

Competing interests

The authors declare no competing interests.

Data and materials availability

All data is available in the manuscript or the supplementary materials.

Materials and Methods

Experimental methods. We collected four different larvacean species (*Bathochordaeus mcnutti, Bathochordaeus stygius, Fritillaria sp., Mesochordaeus erythrocephala*) and conducted in situ high-speed video microscopy of intact internal ciliated ducts to capture ciliary beat kinematics and fluid transport [20]. We also reanalyzed ciliary beat videos we previously recorded in human airway epithelial cultures [86]. To measure ciliated duct morphology, we employed immunofluorescence (IF) imaging of fixed samples of larvaceans and the Hawaiian bobtail squid (*Euprymna scolopes*). Additionally, we collected and analyzed CD morphology from micrographs in literature representing all animal phyla, exclusions applied. The morphometric data sets were analyzed using machine learning to identify the structural parameters most predictive of fluid transport functions (bulk transport or filtration/valving) reported in literature. Complete methods for data acquisition and analysis are provided in Suppl. Materials § S.1

Physics-based modeling. We propose the Brinkman-Stokes equations as an effective model for CDs that bridges the carpet and flame designs and yields a tractable computational framework capable of capturing the essential flow physics in CDs with a minimal number of free parameters. The fluid motion in CDs is characterized by a low Reynolds number $\mathrm{Re} = \rho H U/\mu$, of the order of 10^{-3}–10^{-2}, and is thus governed by the incompressible Stokes equation. To break the time reversibility property of the Stokes equation [95], we considered ciliary waves, consistent with our experimental observations in ciliary carpets and flames (Figs. 1 and S.2) and with existing studies that show that ciliary waves emerge spontaneously and significantly enhance fluid pumping [24–26, 28–31]. Using the Brinkman-Stokes model, we represented the ciliary layers in a coarse-grained fashion as an active porous medium, with prescribed density waves (see, e.g., [92–94]). We solved the resulting equations using an in-house computational fluid dynamics (CFD) solver subject to appropriate boundary conditions (Suppl. Materials, §S.2). For

computational simplicity, we assumed unidirectional ciliary waves, but our Brinkman-Stokes model can be readily generalized to CDs with complex, longitudinal and transverse, waves emerging from non-reciprocal cilia beating and non-uniform cilia distribution (Suppl. Materials, §S.4, Figs. S.15–S.19). Test studies (Figs. S.15–S.19) show that flows resulting from the simpler unidirectional wave approximation capture the salient features of flows resulting from more complicated beating kinematics involving larger number of parameters and higher computational cost.

References

1. Bustamante-Marin, X. M. & Ostrowski, L. E. Cilia and mucociliary clearance. *Cold Spring Harbor Perspectives in Biology* **9,** a028241 (2017).
2. Faubel, R., Westendorf, C., Bodenschatz, E. & Eichele, G. Cilia-based flow network in the brain ventricles. *Science* **353,** 176–178 (2016).
3. Raidt, J. *et al.* Ciliary function and motor protein composition of human fallopian tubes. *Human Reproduction* **30,** 2871–2880 (2015).
5. Tilley, A. E., Walters, M. S., Shaykhiev, R. & Crystal, R. G. Cilia dysfunction in lung disease. *Annual Review of Physiology* **77,** 379–406 (2015).
6. Carter, C. S. *et al.* Abnormal development of NG2+ PDGFR-α+ neural progenitor cells leads to neonatal hydrocephalus in a ciliopathy mouse model. *Nature Medicine* **18,** 1797–1804 (2012).
7. Blyth, M. & Wellesley, D. Ectopic pregnancy in primary ciliary dyskinesia. *Journal of Obstetrics and Gynaecology* **28,** 358–358 (2008).
8. Gilpin, W., Bull, M. S. & Prakash, M. The multiscale physics of cilia and flagella. *Nature Reviews Physics* **2,** 74–88 (2020).
9. McKanna, J. A. Fine structure of the protonephridial system in Planaria. *Zeitschrift für Zellforschung und Mikroskopische Anatomie* **92,** 509–523 (1968).
10. Rink, J. C., Vu, H. T.-K. & Alvarado, A. S. The maintenance and regeneration of the planarian excretory system are regulated by EGFR signaling. *Development* **138,** 3769–3780 (2011).
11. Vu, H. T.-K. *et al.* Stem cells and fluid flow drive cyst formation in an invertebrate excretory organ. *eLife* **4,** e07405 (2015).

12. Vogel, S. Living in a physical world X. Pumping fluids through conduits. *Journal of biosciences* **32,** 207–222 (2007).

4. Yuan, S. *et al.* Motile cilia of the male reproductive system require miR-34/miR-449 for development and function to generate luminal turbulence. *Proceedings of the National Academy of Sciences* **116,** 3584–3593 (2019).

13. Ramirez-San Juan, G. R. *et al.* Multi-scale spatial heterogeneity enhances particle clearance in airway ciliary arrays. *Nature Physics* **16,** 1–7 (2020).

14. Pellicciotta, N. *et al.* Cilia density and flow velocity affect alignment of motile cilia from brain cells. *Journal of Experimental Biology* **223** (2020).

15. Pellicciotta, N. *et al.* Entrainment of mammalian motile cilia in the brain with hydrodynamic forces. *Proceedings of the National Academy of Sciences* **117,** 8315–8325. ISSN: 0027-8424 (2020).

16. Nawroth, J. C. *et al.* A microengineered airway lung chip models key features of viral-induced exacerbation of asthma. *American Journal of Respiratory Cell and Molecular Biology* **63,** 591–600 (2020).

17. Sone, N. *et al.* Multicellular modeling of ciliopathy by combining iPS cells and microfluidic airway-on-a-chip technology. *Science Translational Medicine* **13** (2021).

18. Solari, C. A., Ganguly, S., Kessler, J. O., Michod, R. E. & Goldstein, R. E. Multicellularity and the functional interdependence of motility and molecular transport. *Proceedings of the National Academy of Sciences* **103,** 1353–1358 (2006).

19. Wan, K. Y. & Goldstein, R. E. Coordinated beating of algal flagella is mediated by basal coupling. *Proceedings of the National Academy of Sciences* **113,** E2784–e2793 (2016).

20. Nawroth, J. C. *et al.* Motile cilia create fluid-mechanical microhabitats for the active recruitment of the host microbiome. *Proceedings of the National Academy of Sciences* **114,** 9510–9516 (2017).

21. Kanso, E. A., Lopes, R. M., Strickler, J. R., Dabiri, J. O. & Costello, J. H. Teamwork in the viscous oceanic microscale. *Proceedings of the National Academy of Sciences* **118.** ISSN: 0027-8424 (2021).

22. Gilpin, W., Bull, M. S. & Prakash, M. The multiscale physics of cilia and flagella. *Nature Reviews Physics* **2,** 74–88 (2020).

23. Meng, F., Bennett, R. R., Uchida, N. & Golestanian, R. Conditions for metachronal coordination in arrays of model cilia. *Proceedings of the National Academy of Sciences* **118** (2021).

24. Kanale, A. V., Ling, F., Guo, H., Fürthauer, S. & Kanso, E. Spontaneous phase coordination and fluid pumping in model ciliary carpets. *Proceedings of the National Academy of Sciences* **119,** e2214413119 (2022).

25. Vilfan, A. & Jülicher, F. Hydrodynamic flow patterns and synchronization of beating cilia. *Physical Review Letters* **96,** 058102 (2006).

26. Guirao, B. & Joanny, J.-F. Spontaneous creation of macroscopic flow and metachronal waves in an array of cilia. *Biophysical Journal* **92,** 1900–1917 (Mar. 2007).

27. Narematsu, N., Quek, R., Chiam, K.-H. & Iwadate, Y. Ciliary metachronal wave propagation on the compliant surface of Paramecium cells. *Cytoskeleton* **72,** 633–646 (2015).

28. Han, J. & Peskin, C. S. Spontaneous oscillation and fluid–structure interaction of cilia. *Proceedings of the National Academy of Sciences* **115,** 4417–4422 (2018).

29. Elgeti, J. & Gompper, G. Emergence of metachronal waves in cilia arrays. *Proceedings of the National Academy of Sciences* **110,** 4470–4475 (2013).

30. Ding, Y., Nawroth, J. C., McFall-Ngai, M. J. & Kanso, E. Mixing and transport by ciliary carpets: a numerical study. *Journal of Fluid Mechanics* **743,** 124–140 (2014).

31. Chateau, S., Favier, J., Poncet, S. & d'Ortona, U. Why antiplectic metachronal cilia waves are optimal to transport bronchial mucus. *Physical Review E* **100,** 042405 (2019).

32. Zhang, S., Cui, Z., Wang, Y. & den Toonder, J. Metachronal μ-cilia for on-chip integrated pumps and climbing robots. *ACS applied materials & interfaces* **13,** 20845–20857 (2021).

33. Guo, H., Fauci, L., Shelley, M. J. & Kanso, E. Bistability in the synchronization of actuated microfilaments. *Journal of Fluid Mechanics* **836,** 304–323 (2018).

34. Man, Y. & Kanso, E. Multisynchrony in active microfilaments. *Physical Review Letters* **125,** 148101 (2020).

35. Guo, H., Man, Y., Wan, K. Y. & Kanso, E. Intracellular coupling modulates biflagellar synchrony. *Journal of the Royal Society Interface* **18,** 20200660 (2021).

36. Hildebrandt, F., Benzing, T. & Katsanis, N. Ciliopathies. *New England Journal of Medicine* **364,** 1533–1543 (2011).

37. Andrikou, C., Thiel, D., Ruiz-Santiesteban, J. A. & Hejnol, A. Active mode of excretion across digestive tissues predates the origin of excretory organs. *PLOS Biology* **17,** e3000408 (2019).

38. Ichimura, K. & Sakai, T. Evolutionary morphology of podocytes and primary urine-producing apparatus. *Anatomical Science International* **92,** 161–172 (2017).

39. Essock-Burns, T., Bongrand, C., Goldman, W. E., Ruby, E. G. & McFall-Ngai, M. J. Interactions of Symbiotic Partners Drive the Development of a Complex Biogeography in the Squid-Vibrio Symbiosis. *mBio* **11** (2020).

40. Glover, J. C. Oikopleura. *Current Biology* **30,** R1243–r1245 (2020).

41. Sherlock, R., Walz, K., Schlining, K. & Robison, B. Morphology, ecology, and molecular biology of a new species of giant larvacean in the eastern North Pacific: Bathochordaeus mcnutti sp. nov. *Marine Biology* **164,** 20 (2017).

42. Katija, K. *et al.* Revealing enigmatic mucus structures in the deep sea using DeepPIV. *Nature* **583,** 78–82 (2020).

43. Yang, Z. & Zhang, L. Magnetic actuation systems for miniature robots: A review. *Advanced Intelligent Systems* **2,** 2000082 (2020).

44. Zhang, R., den Toonder, J. & Onck, P. R. Transport and mixing by metachronal waves in nonreciprocal soft robotic pneumatic artificial cilia at low Reynolds numbers. *Physics of Fluids* **33,** 092009 (2021).

45. Islam, T. U. *et al.* Microscopic artificial cilia-a review. *Lab on a Chip* (2022).

46. Meunier, A. & Azimzadeh, J. Multiciliated cells in animals. *Cold Spring Harbor Perspectives in Biology* **8,** a028233 (2016).

47. Holmberg, K. The ciliated brain duct of Oikopleura dioica (Tunicata, Appendicularia). *Acta Zoologica* **63,** 101–109 (1982).

48. Sears, P. R., Yin, W.-N. & Ostrowski, L. E. Continuous mucociliary transport by primary human airway epithelial cells in vitro. *American Journal of Physiology-Lung Cellular and Molecular Physiology* **309,** L99–l108 (2015).

49. Valverde-Islas, L. E. *et al.* Visualization and 3D reconstruction of flame cells of Taenia solium (cestoda). *PLOS One* **6,** e14754 (2011).

50. Olstad, E. W. *et al.* Ciliary beating compartmentalizes cerebrospinal fluid flow in the brain and regulates ventricular development. *Current Biology* **29,** 229–241 (2019).

51. Dunn, C. W., Giribet, G., Edgecombe, G. D. & Hejnol, A. Animal phylogeny and its evolutionary implications. *Annual Review of Ecology, Evolution, and Systematics* **45,** 371–395 (2014).

52. Feuda, R. *et al.* Improved modeling of compositional heterogeneity supports sponges as sister to all other animals. *Current Biology* **27,** 3864–3870 (2017).

53. Asadzadeh, S. S., Larsen, P. S., Riisgård, H. U. & Walther, J. H. Hydrodynamics of the leucon sponge pump. *Journal of the Royal Society Interface* **16,** 20180630 (2019).

54. Leys, S. P. *et al.* The sponge pump: the role of current induced flow in the design of the sponge body plan. *PLOS One* **6,** e27787 (2011).

55. Marshall, W. F., Qin, H., Brenni, M. R. & Rosenbaum, J. L. Flagellar length control system: testing a simple model based on intraflagellar transport and turnover. *Molecular Biology of the Cell* **16,** 270–278 (2005).

56. Ishikawa, H. & Marshall, W. F. Ciliogenesis: building the cell's antenna. *Nature Reviews Molecular Cell Biology* **12,** 222–234 (2011).

57. Scimone, M. L., Srivastava, M., Bell, G. W. & Reddien, P. W. A regulatory program for excretory system regeneration in planarians. *Development* **138,** 4387–4398 (2011).

58. Ruppert, E. E. & Smith, P. R. The functional organization of filtration nephridia. *Biological Reviews* **63,** 231–258 (1988).

60. Taylor, G. Analysis of the swimming of microscopic organisms. *Proceedings of the Royal Society of London. Series A* **209,** 447–461 (1951).

61. Blake, J. Infinite models for ciliary propulsion. *Journal of Fluid Mechanics* **49,** 209–222 (1971).

62. Pak, O. S., Normand, T. & Lauga, E. Pumping by flapping in a viscoelastic fluid. *Physical Review E* **81,** 036312 (2010).

63. Michelin, S. & Lauga, E. Optimal feeding is optimal swimming for all Péclet numbers. *Physics of Fluids* **23,** 101901 (2011).

64. Chrispell, J. C., Fauci, L. J. & Shelley, M. An actuated elastic sheet interacting with passive and active structures in a viscoelastic fluid. *Physics of Fluids* **25,** 013103 (2013).

65. Liron, N. & Mochon, S. The discrete-cilia approach to propulsion of ciliated microorganisms. *Journal of Fluid Mechanics* **75,** 593–607 (1976).

66. Liron, N. Fluid transport by cilia between parallel plates. *Journal of Fluid Mechanics* **86,** 705–726 (1978).

67. Gueron, S. & Liron, N. Ciliary motion modeling, and dynamic multicilia interactions. *Biophysical Journal* **63,** 1045 (1992).

68. Blake, J., Liron, N. & Aldis, G. Flow patterns around ciliated microorganisms and in ciliated ducts. *Journal of Theoretical Biology* **98,** 127–141 (1982).

69. Ding, Y. & Kanso, E. Selective particle capture by asynchronously beating cilia. *Physics of Fluids* **27,** 121902 (2015).

70. Guo, H. & Kanso, E. Evaluating efficiency and robustness in cilia design. *Physical Review E* **93,** 033119 (2016).

71. Guo, H., Zhu, H. & Veerapaneni, S. Simulating cilia-driven mixing and transport in complex geometries. *Physical Review Fluids* **5,** 053103 (2020).

59. Forouhar, A. S. *et al.* The embryonic vertebrate heart tube is a dynamic suction pump. *Science* **312,** 751–753 (2006).

72. Kelly, S. J., Brodecky, V., Skuza, E. M., Berger, P. & Tatkov, S. Variability in tracheal mucociliary transport is not controlled by beating cilia in lambs in vivo during ventilation with humidified and nonhumidified air. *American Journal of Physiology-Lung Cellular and Molecular Physiology* **320,** L473–l485 (2021).

73. Tamori, M., Matsuno, A. & Takahashi, K. Structure and function of the pore canals of the sea urchin madreporite. *Philosophical Transactions of the Royal Society of London. Series B: Biological Sciences* **351,** 659–676 (1996).

74. Ruppert, E. E. Structure, ultrastructure and function of the neural gland complex of Ascidia interrupta (Chordata, Ascidiacea): clarification of hypotheses regarding the evolution of the vertebrate anterior pituitary. *Acta Zoologica* **71,** 135–149 (1990).

75. Bassham, S. & Postlethwait, J. H. The evolutionary history of placodes: a molecular genetic investigation of the larvacean urochordate Oikopleura dioica. *Development* **132,** 4259–4272 (2005).

76. Deyts, C., Casane, D., Vernier, P., Bourrat, F. & Joly, J.-S. Morphological and gene expression similarities suggest that the ascidian neural gland may be osmoregulatory and homologous to vertebrate peri-ventricular organs. *European Journal of Neuroscience* **24,** 2299–2308 (2006).

77. Bartolomaeus, T. & Ax, P. Protonephridia and Metanephridia-their relation within the Bilateria. *Journal of Zoological Systematics and Evolutionary Research* **30,** 21–45 (1992).

78. Ott, E. *et al.* Pronephric tubule morphogenesis in zebrafish depends on Mnx mediated repression of irx1b within the intermediate mesoderm. *Developmental Biology* **411,** 101–114 (2016).

79. Chen, D. & Zhong, Y. A computational model of dynein activation patterns that can explain nodal cilia rotation. *Biophysical Journal* **109,** 35–48 (2015).

80. Dunn, C. W., Leys, S. P. & Haddock, S. H. The hidden biology of sponges and ctenophores. *Trends in Ecology & Evolution* **30,** 282–291 (2015).

81. Leys, S. P. & Eerkes-Medrano, D. I. Feeding in a calcareous sponge: particle uptake by pseudopodia. *The Biological Bulletin* **211,** 157–171 (2006).

82. Norekian, T. P. & Moroz, L. L. Neural System and Receptor Diversity in the ctenophore Beroe abyssicola. *Journal of Comparative Neurology* **527,** 1986–2008 (2019).

83. Tamm, S. L. Cilia and the life of ctenophores. *Invertebrate Biology* **133,** 1–46 (Jan. 2014).

84. Gemmill, J. F. Ciliary action in the internal cavities of the ctenophore Pleurobrachia pileus Fabr. *Proceedings of the Zoological Society of London* **88,** 263–265 (1918).

85. Presnell, J. S. *et al.* The presence of a functionally tripartite through-gut in Ctenophora has implications for metazoan character trait evolution. *Current Biology* **26,** 2814–2820 (2016).

86. Nawroth, J. C., van der Does, A. M., Ryan, A. & Kanso, E. Multiscale mechanics of mucociliary clearance in the lung. *Philosophical Transactions of the Royal Society B* **375,** 20190160 (2020).

95. Purcell, E. M. Life at low Reynolds number. *American Journal of Physics* **45,** 3–11 (1977).

92. Stein, D. B. & Shelley, M. J. Coarse graining the dynamics of immersed and driven fiber assemblies. *Physical Review Fluids* **4,** 073302 (2019).

93. Wuttanachamsri, K. & Schreyer, L. Effects of Cilia Movement on Fluid Velocity: II Numerical Solutions Over a Fixed Domain. *Transport in Porous Media* **134,** 471–489 (2020).

94. Wuttanachamsri, K. & Schreyer, L. Effects of Cilia Movement on Fluid Velocity: I Model of Fluid Flow due to a Moving Solid in a Porous Media Framework. *Transport in Porous Media* **136,** 699–714 (2021).

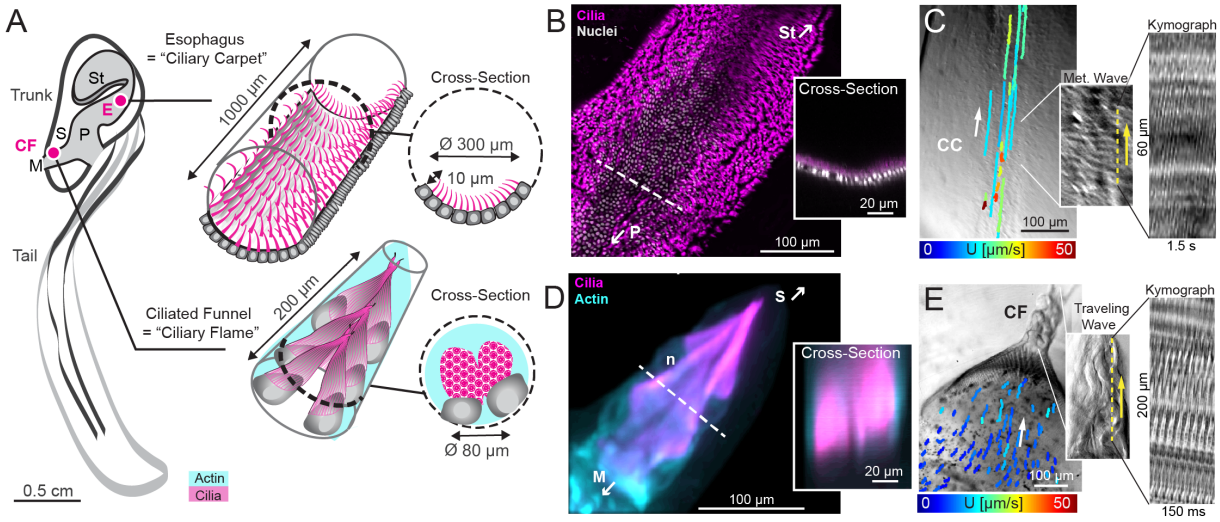

Figure 1: **Comparison of CDs with ciliary flame versus ciliary carpet design in *B. mcnutti* A.** The stomach (St), pharynx (P), and esophagus (E) are lined with ciliary carpets. A ciliated funnel (CF) containing ciliary flame cells connects the mouth (M) cavity to the internal blood sinus (S). **B.** Confocal image of the ciliary carpet of the esophagus (magenta: acetylated α-tubulin). Inset: Horizontal cross section at dotted line. Note that the cilia only fill a small fraction of the lumen. **C.** Direction and magnitude of fluid flow driven by the esophageal ciliary carpet. Insets: Snapshot and kymograph of the esophageal carpet showing metachronal wave and beat frequency of $\sim$20 Hz. Yellow arrow indicates direction of metachronal wave. **D.** Confocal image of the ciliary flame inside the ciliated funnel (magenta: acetylated α-tubulin). Inset: Horizontal cross section at dotted line. Note that the cilia fill a large fraction of the lumen. **E.** Direction and speed of fluid flow converging into the ciliated funnel driven by the ciliary flame. Insets: Snapshot and kymograph of the ciliary flame showing traveling wave and beat frequency of $\sim$60 Hz. Yellow arrow indicates direction of traveling wave.

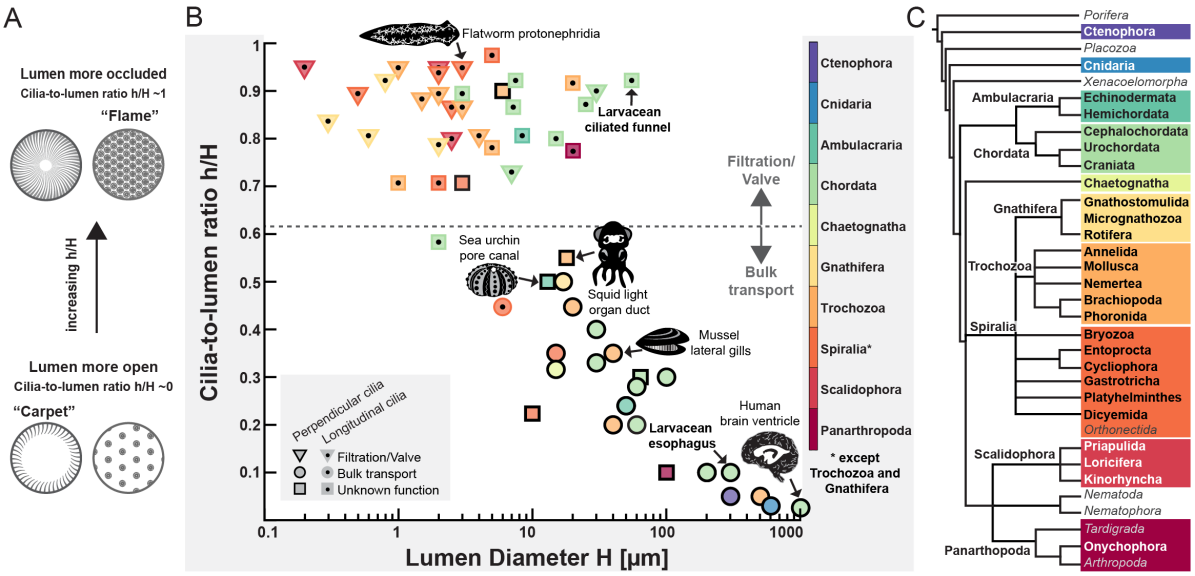

Figure 2: **The morphospace of CDs in nature.** **A.** Cilia-to-lumen ratio h/H describes the relative occlusion of the duct lumen by cilia independent of whether the cilia are oriented perpendicularly (left) or longitudinally (right). Machine learning identified h/H as the best predictor for CD function. Most commonly, but not exclusively, systems with high h/H have longitudinal cilia (flames) and systems with low high h/H have perpendicular cilia (carpets). **B.** CDs plotted based on cilia-to-lumen ratio h/H and lumen diameter H and classified by their functions and phyla (also see Fig. S.5). Triangles ▽ represent systems whose primary functions are thought to be (ultra-) filtration, excretion, or pressure generation. Circles ○ denote systems that transport or mix food particles, liquids, or cells. Squares □ represent systems whose fluid transport functions are currently unknown or disputed. Symbols with solid boundaries are systems with perpendicular ciliation and symbols with a central dot are systems with longitudinal ciliation. The color code indicates the phylogenetic clades listed in the color bar. The dotted line indicates the h/H value identified by machine learning to divide systems with filtration function from systems with bulk transport function. **C.** Phylogenetic tree showing the phyla known to feature CDs and included in the analysis (bold type) and the phyla where CDs are absent, not documented, or shaped in a way that cannot be captured by the morphospace in (B). The color code is the same as in (B). Tree design adapted from [51, 52]

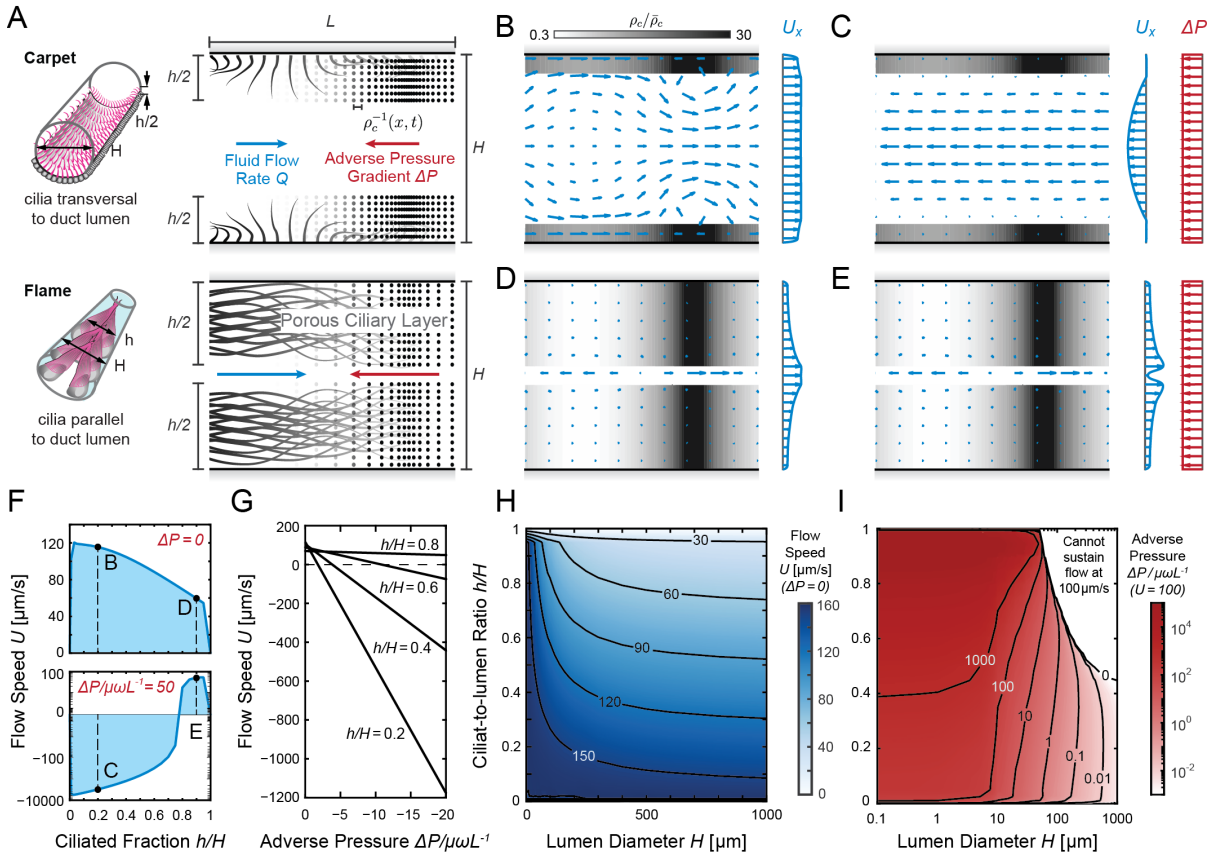

Figure 3: **Computational model that maps CD morphology to fluid pumping.** **A.** Cilia are modeled collectively as an active porous medium with prescribed unidirectional traveling density waves $\rho_c(\mathbf{x}, t)$ at velocity $\boldsymbol{v}(\mathbf{x}, t)$. **B-E.** Computed instantaneous flows $\boldsymbol{u}(\mathbf{x}, t)$ with cross-sectional flow profile $U_x = \int_0^L \boldsymbol{u} \cdot \hat{\mathbf{e}}_x dx$ and net flow speed $U = \int_0^H U_x dy$. Ciliary carpet ($h/H = 0.2$) and flame ($h/H = 0.9$) designs at $\Delta P = 0$ (B and D) and $\Delta P = -50\mu\omega L^{-1}$ (C and E) at which only the flame design pumps fluid in the desired direction. **F.** Flow speed U versus h/H: under large adverse pressure, positive flow is only possible at high cilia-to-lumen ratio. **G.** U versus ΔP: at larger h/H, U decays more slowly as ΔP increases, hence the ability to produce positive flow at larger adverse pressure. **H.** Flow speed U over the entire morphospace (H, h/H) at $\Delta P = 0$. **I.** Adverse pressure gradients ΔP for which a net flow speed of $U = 100$ μm s^{-1} is achievable. Contour lines indicate that flame designs continue to pump as ΔP increases. In all panels, $\bar{\rho}_c h = 1000$, $\omega = 20$ Hz and $L = 100$ μm, and in panels A–C, $H = 100$ μm.

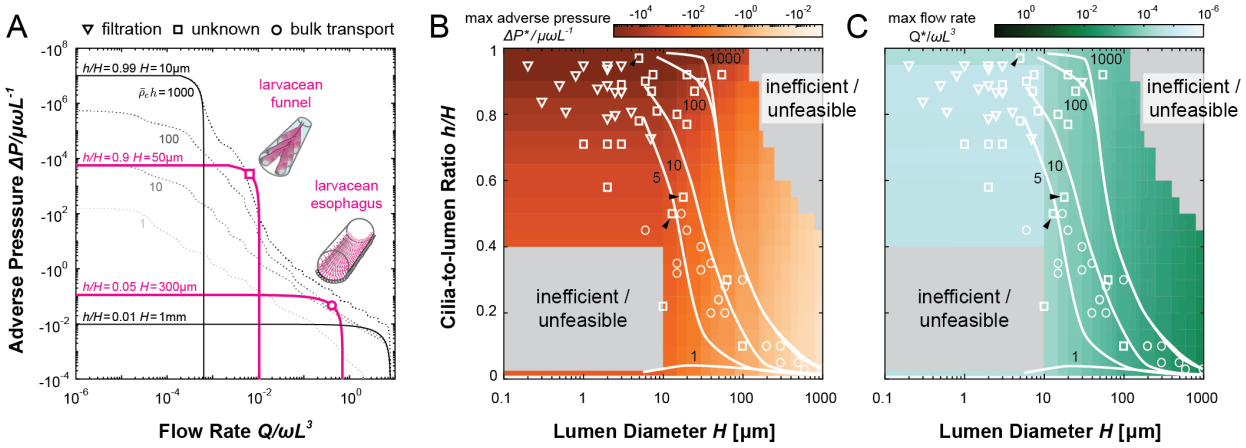

Figure 4: **Optimal CD designs.** **A.** Pumping performance of two extreme CD design (solid black lines, $\bar{\rho}_c h = 1000$), and the larvacean ciliated funnel ($\bar{\rho}_c h = 200$) and esophagus ($\bar{\rho}_c h = 40$). Flow rates and adverse pressures that maximize pumping efficiency η at different ciliary material constants $\bar{\rho}_c h = 1, 5, 10, 100, 1000$ are superimposed (dotted curves). **B-C.** Optimal CD morphologies in the $(H, h/H)$ morphospace (white lines) exhibit a shift from carpet to flame designs at larger values of maximum adverse pressure (orange colormap), accompanied by a decrease in optimal flow rate (green colormap). Biological data from Fig. 2A are superimposed with biological function: bulk transport ○, filtration ▽, and unknown □. Grey regions indicate sub-optimal designs (efficiency $< 50\%$; see Fig. S.14).